

The BANANA Project. VII. High Eccentricity Predicts Spin-Orbit Misalignment in Binaries

MARCUS L. MARCUSSEN ^{1,2} SIMON H. ALBRECHT ^{1,2} JOSHUA N. WINN ² YUBO SU ² MIA S. LUNDKVIST ¹ AND
KEVIN C. SCHLAUFMAN ³

¹*Department of Physics and Astronomy, Aarhus University, Ny Munkegade 120, 8000 Aarhus C, Denmark*

²*Department of Astrophysical Sciences, Peyton Hall, 4 Ivy Lane, Princeton, NJ 08544, USA*

³*William H. Miller III Department of Physics & Astronomy, Johns Hopkins University, 3400 N Charles St, Baltimore, MD 21218, USA*

ABSTRACT

The degree of spin-orbit alignment in a population of binary stars can be determined from measurements of their orbital inclinations and rotational broadening of their spectral lines. Alignment in a face-on binary guarantees low rotational broadening, while alignment in an edge-on binary maximizes the rotational broadening. In contrast, if spin-orbit angles (ψ) are random, rotational broadening should not depend on orbital inclination. Using this technique, we investigated a sample of 2,727 astrometric binaries from Gaia DR3 with F-type primaries and orbital periods between 50 and 1000 days (separations 0.3–2.7 au). We found that ψ is strongly associated with e , the orbital eccentricity. When $e < 0.15$, the mean spin-orbit angle is $\langle\psi\rangle = 6.9_{-4.1}^{+5.4}$ degrees, while for $e > 0.7$, it rises to $\langle\psi\rangle = 46_{-24}^{+26}$ degrees. These results suggest that some binaries are affected by processes during their formation or evolution that excite both orbital eccentricity and inclination.

1. INTRODUCTION

Stellar spin-orbit angles (also called obliquities) are affected by processes that take place during the formation and evolution of binary stars. Binaries that formed via disk fragmentation are expected to have well-aligned rotational and orbital axes. However, numerous processes can misalign a binary, such as chaotic accretion during the star formation process (Bate et al. 2010; Thies et al. 2011; Fielding et al. 2015; Offner et al. 2016; Bate 2018; Jennings & Chiang 2021), torques from a warped circumbinary disk (Anderson & Lai 2021), close encounters with other stars in the birth cluster (e.g. Heggie & Rasio 1996; Rodet et al. 2021), and Kozai-Lidov cycles caused by a distant third star (e.g. Mazeh & Shaham 1979; Eggleton & Kiseleva-Eggleton 2001; Fabrycky & Tremaine 2007; Naoz & Fabrycky 2014; Anderson et al. 2017).

However, there are relatively few observational constraints on spin-orbit alignment in binaries. Most existing measurements of spin-orbit angles are not for the spins of stars with respect to binary orbital planes, but rather for the spins of stars relative to the plane of a *planetary orbit* (Albrecht et al. 2022). The aim of project BANANA (Binaries Are Not Always Neatly

Aligned) is to measure the obliquities of stars in binary systems and thereby constrain theories of binary formation and evolution. For the close double star systems DI Herculis and CV Vel, we found that all four stars have large obliquities (Albrecht et al. 2009, 2014a). We have also found some systems to be closely aligned (Albrecht et al. 2007, 2011, 2013, 2014b; Marcussen & Albrecht 2022). We refer the reader to Pavlovski et al. (2011); Triaud et al. (2013); Lehmann et al. (2013); Philippov & Rafikov (2013); Zhou & Huang (2013); Sybilski et al. (2018) and Ball et al. (2023) for descriptions of similar efforts by other groups to measure spin-orbit angles in close binaries.

Spin-orbit alignment has also been studied in wider binaries, with separations exceeding 1 au (see, e.g., Weis 1974; Hale 1994; Glebocki & Stawikowski 1997; Howe & Clarke 2009; Justesen & Albrecht 2020). However, Justesen & Albrecht (2019) showed that with the data at hand, it is still too early to draw firm conclusions about spin-orbit angles in wide binaries. See Offner et al. (2023) for a recent review on multiple star formation and measurements of the angles between protostars and their disks.

Here we present a study of spin-orbit alignment in a population of several thousand wide binaries that were selected from Data Release 3 (DR3) of the Gaia mission (Gaia Collaboration et al. 2021). For reasons relating to our technique, described below, the sample is restricted

to single-lined binaries with F-type primaries and orbital periods ranging from 50 to 1000 days. Our technique builds on previous work by many others (e.g. Weis 1974; Hale 1994; Schlaufman 2010; Masuda & Winn 2020; Louden et al. 2021), in that we rely on observations of rotational broadening of spectral lines. The $\sin i$ dependence of rotational broadening can be used to extract statistical information about the orientation distribution of a population of stars. We combine this information with orbital inclinations derived from astrometric data to arrive at constraints on the distribution of spin-orbit angles.

Section 2 describes our selection of Gaia DR3 binaries. Section 3 compares the spectral line broadening observed for face-on binaries and edge-on binaries. A significant difference was found — implying low obliquities — but only for binaries with relatively low orbital eccentricities ($e \lesssim 0.5$). Section 4 describes our “forward-modeling” method for deriving quantitative constraints on the obliquity distribution. Section 5 displays the results of this method, and Section 6 discusses possible implications for theories of binary formation and dynamics. We also highlight future directions of research using this technique.

2. SAMPLE

This work is based on the catalog of astrometric binaries that accompanied Gaia DR3 (Gaia Collaboration et al. 2022). For all of the binaries, the Keplerian orbital elements were determined by fitting the time-series astrometric data. The astrometry-only solutions are labelled `Orbital` in the Non-Single Source Gaia DR3 table (Gaia Collaboration et al. 2022). All of the binaries were also observed with Gaia’s Radial Velocity Spectrometer (RVS) and a subset were found to be single-lined binaries; for those systems, data are available from the joint astrometric and spectroscopic solutions, `AstroSpectroSB1`.

For our study, a key parameter from Gaia DR3 is the `vbroad` parameter (Frémat et al. 2023), which quantifies the observed spectral-line broadening of the primary star. As we will show below, for most F-type stars, the broadening is dominated by rotational line broadening, allowing for the calibration of a relationship between `vbroad` and the projected rotation velocity $v \sin i$, where i is the inclination of the stellar rotation axis. The sample we study includes only single-lined binaries, for which the observed flux comes mainly from the primary star. The tabulated `vbroad` parameter can therefore safely be attributed to the primary star. Thus, in what follows, when we refer to spin-orbit alignment, we mean

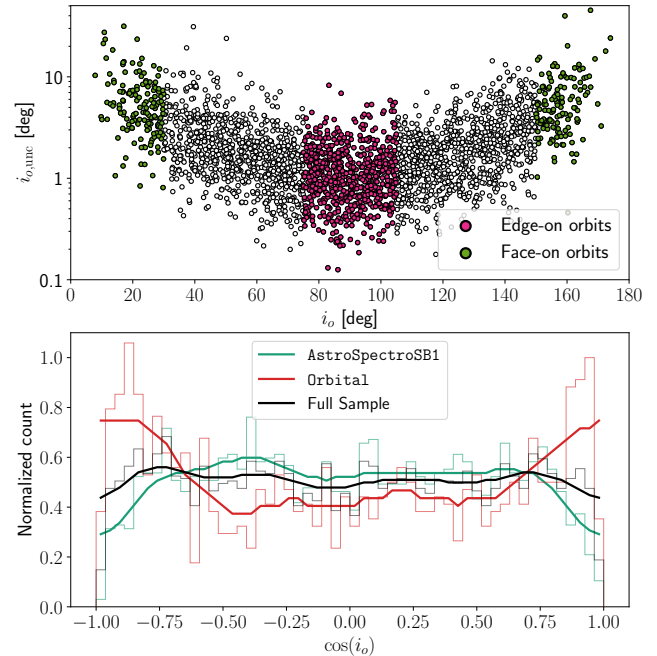


Figure 1. Orbital inclinations i_o of binaries in the sample. *Top:* Values and uncertainties of i_o from Gaia DR3. We classified the binaries as “edge-on” (pink points), “face-on” (green points) or intermediate (white points). *Bottom:* Distribution of $\cos i_o$ of stars for which SB1 solutions are available in addition to astrometry (`AstroSpectroSB1`) and stars for which only astrometric data are available (`Orbital`). An isotropic distribution of orientations would lead to a uniform distribution in $\cos i_o$.

the alignment between the spin axis of the *primary* star and the axis of the binary orbit.

We imposed several selection criteria to create a relatively homogeneous and high-quality sample. We started with systems for which the G_{RVS} magnitude is brighter than 12 because the `vbroad` parameter is not available for fainter stars. We required the reported uncertainty in `vbroad` to be less than 10 km s^{-1} . We restricted the range of orbital periods to be between 50 and 1000 days. We omitted stars with unusually low or high surface gravity or metallicity. Specifically, we restricted $\log g$ to the range between 3.8 and 4.5 and metallicity $[M/H]$ to the range between -1 and 1 . We required the effective temperature T_{eff} to be between 6000 K and 7000 K, roughly corresponding to F-type stars, and we also required the uncertainty to be smaller than 100 K. Main sequence stars with lower effective temperatures tend to rotate too slowly to allow for reliable observations of rotational broadening with the RVS. For stars hotter than ~ 7000 K, Frémat et al. (2023) found the `vbroad` parameter to be an unreliable measure of rotational broadening. Finally, we required the “signifi-

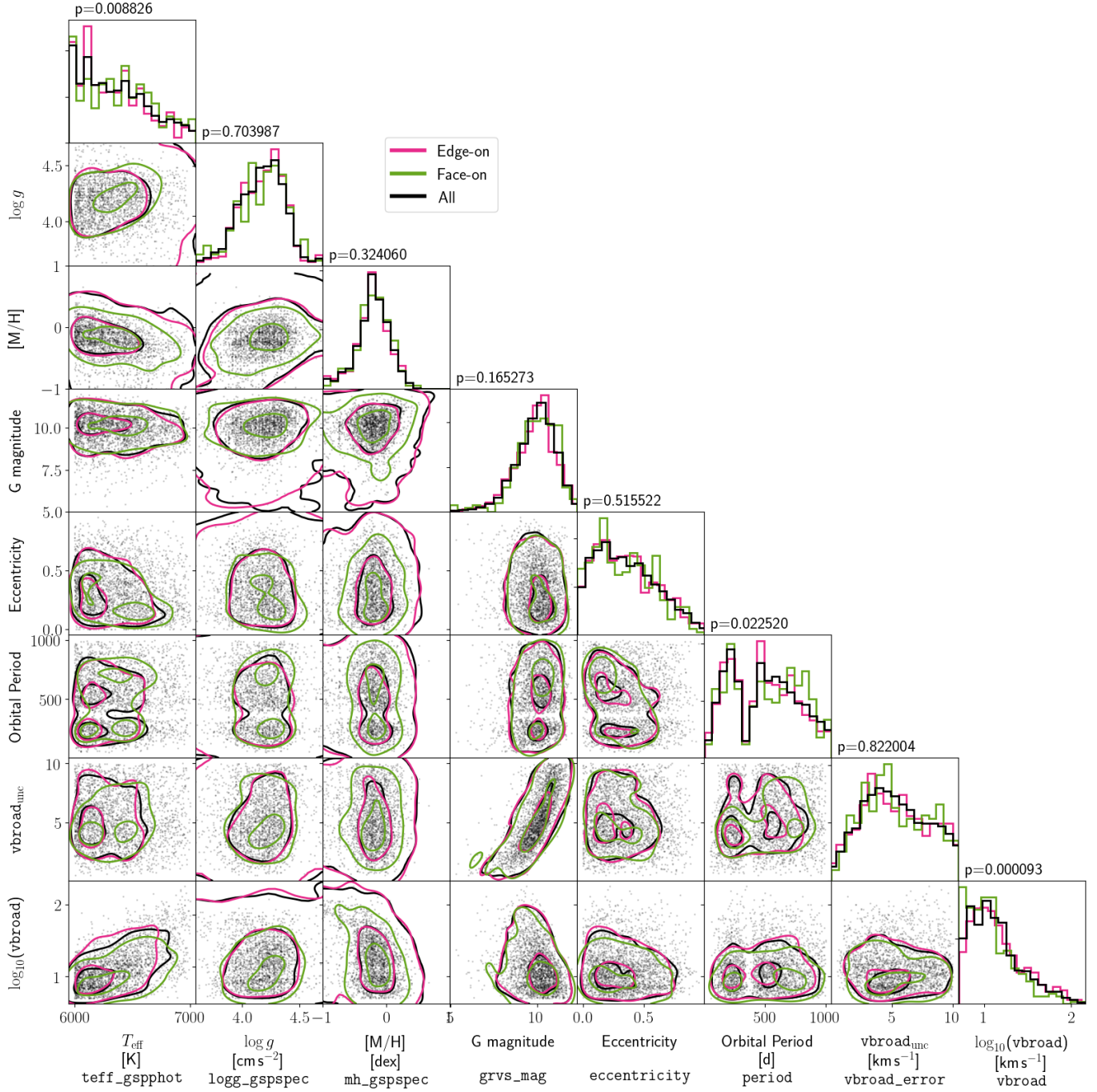


Figure 2. Physical parameters of the binary sample. A selection of relevant parameters and their correlations are shown for the full sample of binary systems (black) and for the face-on and edge-on subsets (green and pink). The p -values printed above the histograms come from KS tests comparing the edge-on and face-on samples.

“cance” parameter s associated with the astrometric solution to exceed 5. Roughly speaking, the s parameter is the signal-to-noise ratio (Halbwachs et al. 2023). A total of 2,727 systems satisfied all of our criteria, which are summarized as:

$$\begin{aligned} \text{vbroad}_{\text{unc}} &< 10 \text{ km s}^{-1} \\ 50 \text{ d} &< \text{orbital period} < 1000 \text{ d} \\ 3.8 &< \log g < 4.5 \\ -1 &< [M/H] < 1 \\ 6000 \text{ K} &< T_{\text{eff}} < 7000 \text{ K} \\ T_{\text{eff,unc}} &< 100 \text{ K} \\ 5 &< \text{significance } s \text{ of astrometric solution} \end{aligned}$$

The top panel of Figure 1 shows the orbital inclinations of this sample, which we obtained by transforming the tabulated Thiele-Innes elements into Campbell elements (Gaia Collaboration et al. 2022). Not surprisingly, the uncertainties tend to be larger when the orbit is nearly face-on. The bottom panel shows the distributions of $\cos i_o$ for the *AstroSpectroSB1* binaries and for the *Orbital* binaries. The *AstroSpectroSB1* contains relatively few face-on orbits, as expected, since a low inclination implies low radial velocities. The distribution of $\cos i_o$ is close to uniform for all the binaries (i.e. the joint sample of *Orbital* and *AstroSpectroSB1*), corresponding to an isotropic distribution of orientations in three dimensions.

We classified each of the 2,727 systems based on orbital inclination. “Edge-on” systems have inclinations between 75° and 105° . “Face-on” systems have inclinations that are either between 0° and 30° or between 150° and 180° . With these definitions, the sample contains 686 edge-on systems and 296 face-on systems. The remaining 1,745 systems have intermediate inclinations (see top panel of Figure 1).

Figure 2 shows the distributions of many other parameters in the full sample as well as the face-on and edge-on subsets. In order for a difference in line-broadening between the two subsets to be attributed to a difference in stellar inclination, the intrinsic rotation velocity of the two samples must be the same. While the rotation speed should not depend on the direction from which a system is viewed, differences in detectability may arise due to other astrophysical parameters influencing the photometric or spectroscopic data. If the rotation speed depends on any of these parameters, and if their distributions vary between edge-on and face-on systems, a systematic difference in rotation speed between the samples might still occur. Although the parameter distributions for the edge-on and face-on subsets look similar,

Kolmogorov–Smirnov (KS) tests revealed three parameters for which the null hypothesis that the values in the edge-on and face-on subsets are drawn from the same distribution is unlikely ($p < 0.05$).

The first case is the effective temperature ($p = 0.0088$). The edge-on systems show a peak in the temperature distribution near 6150 K. This may be an effect of discrete sampling used for the parameter inference in DR3, resulting in some parameters not being smoothly distributed. These discrete sampling effects, showing artificial over densities or under densities, are evident in the distributions of several parameters in our sample, as shown in Figure 2. Regardless of the origin of this difference near 6150 K, it appears minor and is probably irrelevant to the subsequent analysis, where we attempted to control for effective temperature.

The second case is the orbital period, where the face-on sample has more weight at longer periods than the full sample ($p = 0.02$). We hypothesize that this is because, all other things being equal, astrometric characterization is easier for face-on orbits than edge-on orbits. For example, the uncertainties in orbital eccentricity and inclination are more strongly correlated for edge-on orbits compared to face-on orbits. If this is so, then DR3 would contain more orbital solutions for face-on systems than edge-on systems — especially when the period approaches the maximum detectable period, inhibiting detection. Although we cannot be sure of this explanation, we assume that the difference in period distributions does not matter for our analysis, since *vbroad* and period are not detectably correlated (see Figure 2).

The final and most interesting case of a parameter whose distributions in the edge-on and face-on samples appears statistically different is *vbroad* ($p = 9.3 \times 10^{-5}$). The face-on systems tend to have lower values of *vbroad* than either the complete sample or the edge-on sample. Another way to express the difference between the *vbroad* distributions of the edge-on and face-on samples is to examine the mean values and the standard errors in the mean. For the edge-on systems, $\langle \text{vbroad} \rangle_{\text{edge}} = 19.03 \pm 0.70 \text{ km s}^{-1}$, while for the face-on systems, $\langle \text{vbroad} \rangle_{\text{face}} = 14.20 \pm 0.73 \text{ km s}^{-1}$, a $4.8\text{-}\sigma$ difference. In the full sample, $\langle \text{vbroad} \rangle_{\text{all}} = 17.49 \pm 0.32 \text{ km s}^{-1}$.

The overall trends are that the face-on systems show narrower lines than the edge-on systems, and the edge-on systems show slightly wider lines than the full sample. These trends are just what would be expected if the directions of the spin and orbital axes were correlated, and it would be unexpected if the directions were uncorrelated.

3. DEPENDENCE ON EFFECTIVE TEMPERATURE AND ECCENTRICITY

The next step in our analysis was to investigate this result in more detail by testing for any dependence on effective temperature and orbital eccentricity. Figure 3 illustrates these investigations.

The top panel shows the distribution of vbroad for the full sample and for the two subsamples. Compared to the edge-on sample, the face-on sample has more vbroad values below 10 km s^{-1} , and fewer values of higher line broadening. The mean and median values of the distributions are also indicated.

The second panel from the top shows a different line of evidence for systematically low values of vbroad in the face-on sample, based on the fact that the Gaia team chose not to report vbroad whenever it was found to be smaller than 5 km s^{-1} . Because of this choice, the fraction of systems for which vbroad is reported is an indicator of how many systems have low vbroad values. The plot shows this fraction as a function of effective temperature. Compared to the full sample, the fraction of systems for which vbroad was reported is lower for face-on systems and higher for edge-on systems, across all effective temperatures, indicative of spin-orbit alignment. For this plot, the systems were chosen with the same criteria as in the full sample except for the criteria relating to vbroad and its uncertainty.

The rotation velocities of main-sequence stars have long been known to be a strong function of effective temperature (Kraft 1967). Hotter and more massive stars rotate faster, with an especially sharp rise over the temperature range from 6,000 K to 7,000 K considered in our study. We might therefore expect to see an even clearer difference in the distributions of vbroad between face-on and edge-on binaries if we only compare stars with similar effective temperatures. Such a difference can be seen in the third panel from the top in Figure 3. Across the entire range of effective temperatures, face-on systems have a lower mean value of vbroad than do edge-on systems. To control for this temperature dependence, we defined a star’s “normalized” value of vbroad , denoted $\langle \text{vbroad} \rangle$, to be vbroad divided by the mean vbroad for stars of the same effective temperature. The mean vbroad for a given temperature was calculated by linearly interpolating between the temperature-binned mean vbroad values, represented by black, horizontal lines in the 3rd panel of Figure 3.

The bottom panel of Figure 3 shows evidence that the difference in the vbroad distributions of face-on and edge-on subsets is most pronounced for binaries with low eccentricities, and is low or non-existent for binaries with $e > 0.7$. To make this plot, we grouped the bina-

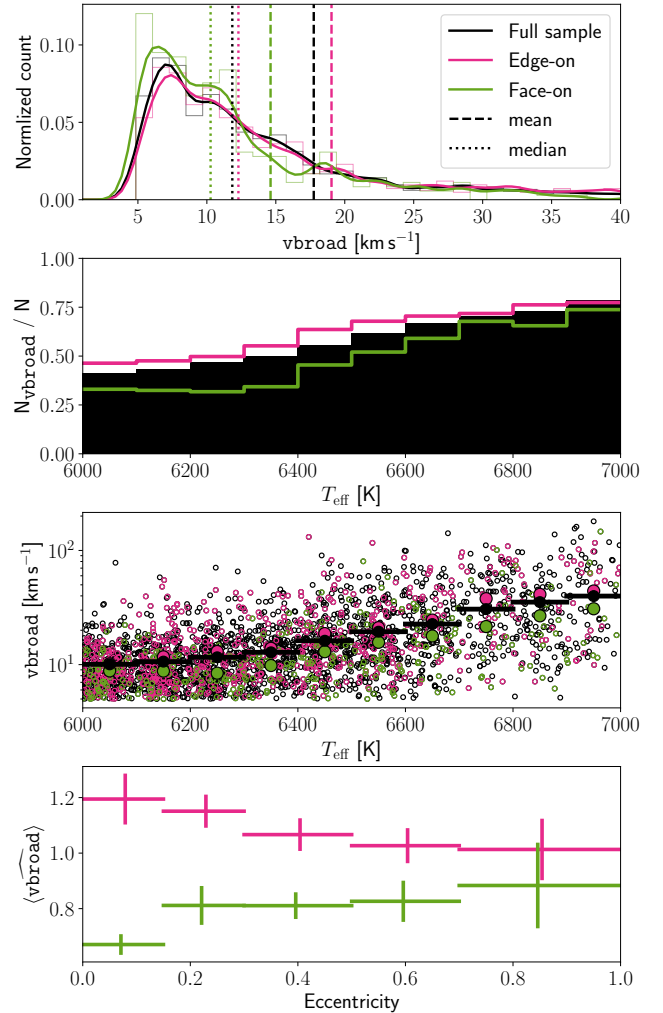


Figure 3. Observed differences in vbroad between face-on and edge-on binaries.

1st panel: Smoothed and normalized histograms of the Gaia line-broadening parameter vbroad for all binaries in the sample, as well as for the edge-on or face-on subsamples. *2nd panel:* Fraction of systems for which vbroad exceeds 5 km s^{-1} or, more literally, the fraction for which vbroad was reported in Gaia DR3. This fraction is shown for the edge-on systems, face-on systems, and the full sample separately, and was split into temperature bins of 100 K. *3rd panel:* vbroad as a function of T_{eff} . The mean vbroad values of stars in 100 K bins are also shown. Across all temperatures, the edge-on sample shows systematically higher values of vbroad , and vice versa for the face-on sample, indicative of spin-orbit alignment. *Bottom panel:* The mean value of $\langle \text{vbroad} \rangle$, the factor by which vbroad exceeds the mean value of all stars of the same effective temperature. This is shown as a function of orbital eccentricity. Horizontal lines indicate the width of the eccentricity bins, and vertical lines indicate the uncertainty. Evidently, nearly-circular binaries exhibit stronger spin-orbit alignment than highly eccentric binaries.

ries into five bins according to orbital eccentricity and computed the mean $\overline{v_{\text{broad}}}$ of the binaries in each bin, a quantity we denote as $\langle v_{\text{broad}} \rangle$. We did this entire process separately for the edge-on systems and the face-on systems. The plot shows that the primary stars of low-eccentricity, low-inclination binaries have systematically narrower spectral lines than the primary stars in low-eccentricity, high-inclination binaries. This systematic difference progressively declines as binaries with higher eccentricities are considered, suggesting that eccentricity and spin-orbit alignment are correlated quantities.

4. INFERRING THE OBLIQUITY DISTRIBUTION

To go beyond testing for statistical differences and derive quantitative constraints on the obliquity distribution, we used a forward-modeling approach. We constructed synthetic v_{broad} distributions through a Monte Carlo procedure, starting with a hypothesized obliquity distribution and simulating the relevant observational effects. We then determined the ranges of the parameters of the hypothesized obliquity distribution that bring the synthetic distributions into agreement with the measured v_{broad} distributions. Before this was possible, we needed to solve two problems:

- We needed to calibrate the relationship between v_{broad} and $v \sin i$. Section 4.1 describes our calibration method.
- We needed a good model for the distribution of stellar rotation velocities as a function of effective temperature. Section 4.2 presents our model.

4.1. Relationship between v_{broad} and $v \sin i$

The v_{broad} parameter in Gaia DR3 was obtained by modeling the observed spectral lines under the assumptions that the star is single and the only broadening mechanism is rotation (Frémat et al. 2023). Other broadening effects such as turbulent convection and pressure broadening were not modeled. Even in the absence of those other effects, imperfect modeling of instrumental broadening can cause v_{broad} to differ from $v \sin i$. Additionally, as mentioned above, whenever v_{broad} was found to be smaller than 5 km s^{-1} , it was not reported in DR3. We needed a model that predicts, as a function of $v \sin i$, both the value of v_{broad} and the probability that v_{broad} would be reported in Gaia DR3.

As a starting point, we conducted spectroscopic observations of bright F-type stars in order to measure $v \sin i$ with higher spectral resolution than the Gaia RVS instrument. We obtained spectra with a signal-to-noise ratio of about 80 and a spectral resolution of about 67 000

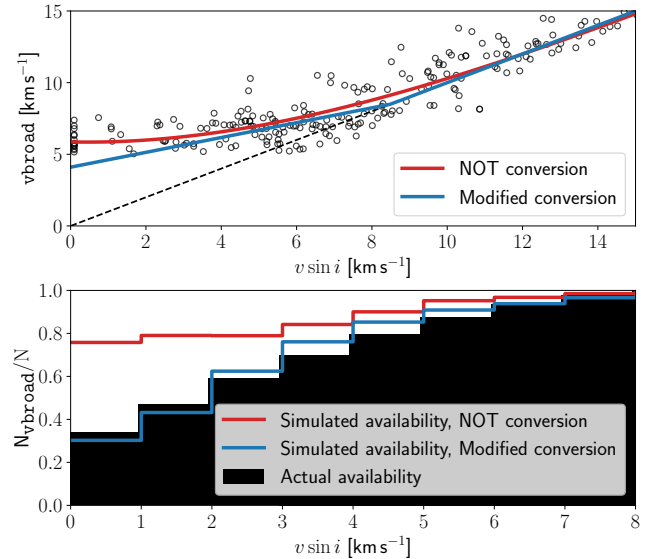


Figure 4. Relationship between v_{broad} and $v \sin i$ based on our FIES calibration sample. The top panel shows v_{broad} and $v \sin i$ for 203 stars. The dashed black line is the identity line. The red curve shows a simple fit to the data, and the blue curve is our adopted relationship (see Equation 1). The black histogram in the bottom panel shows the fraction of all the stars we observed with the NOT for which v_{broad} was reported in Gaia DR3 (and therefore exceeds 5 km s^{-1}). The red and blue histograms are based on simulations employing the red and blue calibration curves depicted in the top panel.

(nearly six times higher than the RVS) using the FIES spectrograph at the Nordic Optical Telescope (Djupvik & Andersen 2010). We measured $v \sin i$ with the iSpec tool (Blanco-Cuaresma et al. 2014). We observed 279 systems for which $v \sin i$ turned out to be below 15 km s^{-1} , with results shown in Figure 4. Of these 279 systems, there were 203 for which v_{broad} was reported in Gaia DR3. As expected, the frequency with which v_{broad} was reported is lower for the lower- $v \sin i$ systems; see the black histogram in Figure 4. The manner in which the frequency declines depends on the relationship between v_{broad} and $v \sin i$. We took advantage of this fact by adjusting our calibration relationship until the simulations agreed with the observations. The bottom panel of Figure 4 shows a comparison between the data and our simulations of the “availability frequency” of v_{broad} as a function of $v \sin i$. Based on these considerations, the formula we adopted to calculate v_{broad} (in km s^{-1}) based on $v \sin i$ was:

$$v_{\text{broad}} = \begin{cases} 4.1 \left(1 - \frac{x}{8.5}\right), & \leq x \leq 8.5 \\ x, & x > 8.5, \end{cases} \quad (1)$$

Parameter	Value
k	0.197 ± 0.003
a_m	$0.017 \pm 0.0009 \text{ km s}^{-1}$
a_s	$26.0 \pm 1.6 \text{ km s}^{-1}$
b_s	$21.9 \pm 0.46 \text{ km s}^{-1}$
c_s	$21.4 \pm 0.78 \text{ km s}^{-1}$

Table 1. Parameters describing the overall v distribution in our binary star sample used in Equation 2.

where x is $v \sin i$ expressed in km s^{-1} . This formula is shown as a blue curve in Figure 1. The red curve is a polynomial fit between $\mathbf{v}\mathbf{b}\mathbf{r}\mathbf{o}\mathbf{a}\mathbf{d}$ and $v \sin i$, which appears to be a good fit but does not correctly reproduce the fraction of systems for which $\mathbf{v}\mathbf{b}\mathbf{r}\mathbf{o}\mathbf{a}\mathbf{d}$ is reported (and therefore for which it is lower than 5 km s^{-1}). We have reported on this calibration procedure for completeness. However, since we could not be sure that the F-type stars we observed with FIES spanned the same range of masses and ages as the primary stars in our sample of astrometric binaries, and out of concern that stars in binaries might have systematically different rotation velocities than field stars, we ultimately decided to use the parameters of this FIES-based calibration only as initial guesses for the parameters in the more flexible model described below.

4.2. Model for rotation velocity

In our simulations, we needed to assign a rotation velocity to each star. Many “gyrochronological” relationships have been established between mass, age, and rotation velocity, but none were derived for binaries with our chosen characteristics. Instead, we posited a simple stochastic function to describe the dependence on effective temperature of both the mean rotation velocity and the spread in rotation velocities:

$$v(T_{\text{eff}}) = v_{\text{min}}(T_{\text{eff}}) + v_{\text{scat}}(T_{\text{eff}})[\mathcal{U}(0, 1)^{-k} - 1], \quad (2)$$

where

$$v_{\text{min}}(T_{\text{eff}}) = a_m(T_{\text{eff}} - 6000 \text{ K}) \quad (3)$$

$$v_{\text{scat}}(T_{\text{eff}}) = a_s + b_s(T_{\text{eff}} - 6250 \text{ K}) + c_s(T_{\text{eff}} - 6250 \text{ K})^2 \quad (4)$$

Here, $\mathcal{U}(0, 1)$ is a random number drawn from a uniform distribution between 0 and 1, v_{min} is the minimum rotation velocity, and v_{scat} is the scatter in the velocity distribution. The scatter might arise from the stochastic nature of star formation and evolution as well as variation in other stellar parameters such as surface gravity and metallicity. If the stars strictly obeyed the Skumanich Law ($v \propto \tau^{-1/2}$) and their ages were drawn ran-

domly from a uniform distribution, then k would have a value of 0.5.

To find the best-fit values for the parameters k , a_m , a_s , b_s , and c_s , we needed a sample of systems for which the distribution of stellar inclinations is known. For this purpose, we assumed that the stellar spin axes in our entire sample of binaries have directions drawn from an isotropic distribution. This seemed safe because the orbital inclinations are observed to have a nearly isotropic distribution, and if so, then the stellar inclinations should also be isotropically distributed, irrespective of the underlying degree of spin-orbit alignment. We also assumed that v depends only on effective temperature, and that a single function $v(T_{\text{eff}})$ is applicable to all stars in the sample.

To assess the agreement between the observed and simulated $\mathbf{v}\mathbf{b}\mathbf{r}\mathbf{o}\mathbf{a}\mathbf{d}$ distributions, we defined a similarity metric based on the means and widths of the distribution of $\mathbf{v}\mathbf{b}\mathbf{r}\mathbf{o}\mathbf{a}\mathbf{d}$ for the primary stars in each of four T_{eff} bins. These bins spanned 250 K each. Specifically, the following statistic was minimized:

$$\chi^2 = \sum_{i=1}^4 \left(\frac{\mu_{\text{sim}, T_i} - \mu_{\text{real}, T_i}}{\text{SE}_\mu} \right)^2 + \quad (5)$$

$$\sum_{i=1}^4 \left(\frac{\sigma_{\text{sim}, T_i} - \sigma_{\text{real}, T_i}}{\text{SE}_\sigma} \right)^2, \quad (6)$$

where T_i refers to the i th temperature bin,¹ μ is the mean value of $\mathbf{v}\mathbf{b}\mathbf{r}\mathbf{o}\mathbf{a}\mathbf{d}$, and SE_μ and SE_σ refer to the standard error of the mean and standard deviations, respectively. The binned $\mathbf{v}\mathbf{b}\mathbf{r}\mathbf{o}\mathbf{a}\mathbf{d}$ distributions are shown in different colors in Figure 5. The optimal parameters were found by minimizing χ^2 , and the parameter uncertainties were found by perturbing each parameter away from the optimal value until χ^2 increased by one unit.

The optimal parameter values are given in Table 1. The resulting functions for v_{scat} and v_{min} are also shown in green in the top left panel of Figure 5.

4.3. Obliquity distribution and resulting stellar inclinations

As a simple parametric model for the distribution of stellar obliquities, we decided to follow Fabrycky & Winn (2009) and use the von-Mises Fisher (VMF) distribution,

$$p(\psi) = \frac{\kappa}{2 \sinh \kappa} \exp(\kappa \cos \psi) \sin \psi. \quad (7)$$

This distribution resembles a 2-d Gaussian distribution wrapped around a sphere. The degree of spin-orbit

¹ For clarity we dropped the subscript “eff” for temperature in these equations.

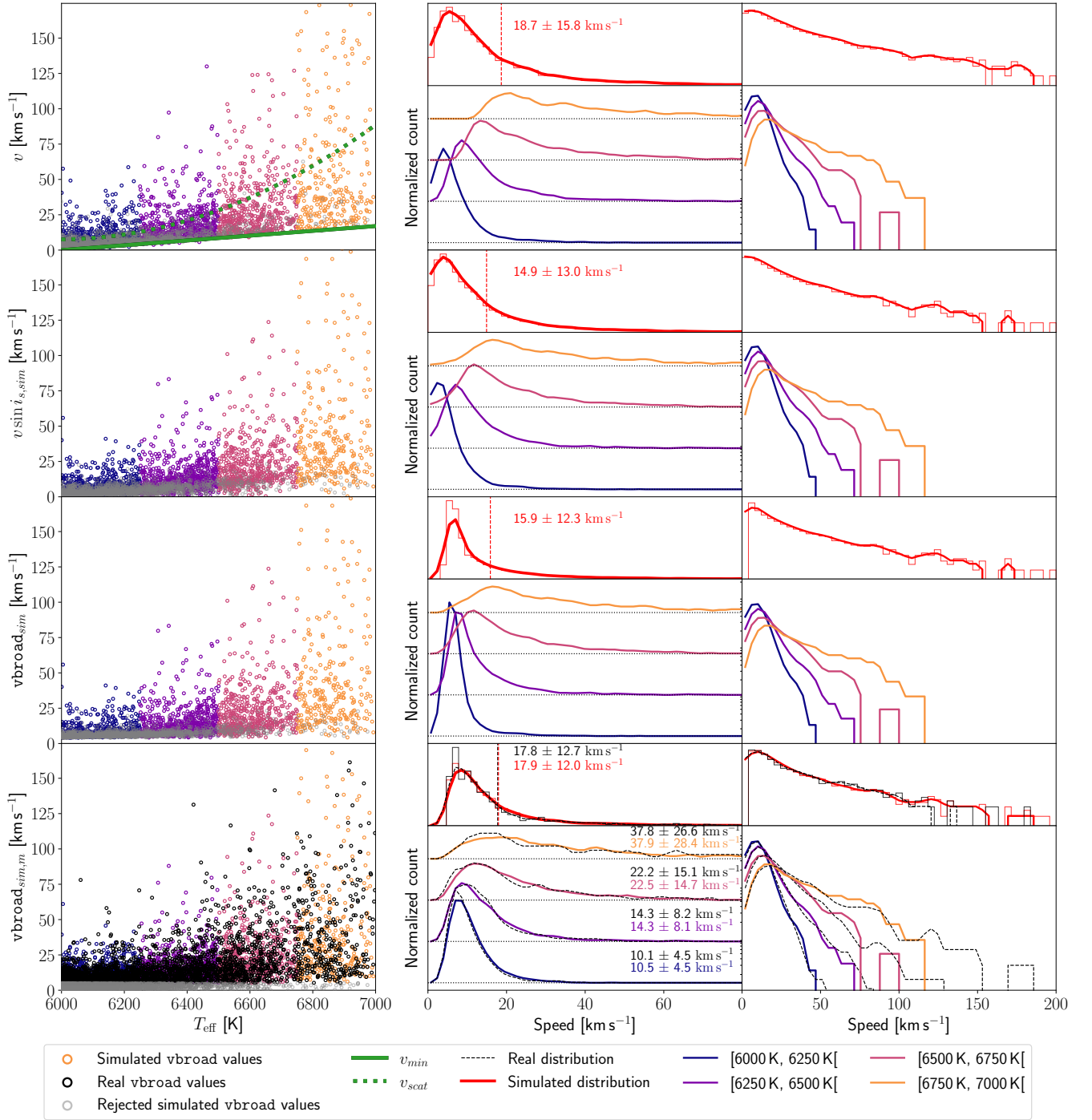


Figure 5. Empirical calibration of rotation speed and v_{broad} . This 4 × 3 grid of panels illustrates the steps in our model relating v , v_{broad} , and effective temperature. The first row shows simulated rotation speeds v , with the first column displaying the distribution of values, and the second & third columns showing histograms on linear & logarithmic scales. Also shown are the best-fit functions for v_{min} and v_{scat} . The second row shows simulated $v \sin i$ values, assuming isotropic orientations. The third row shows the corresponding values of v_{broad} using our conversion formulas. The fourth row shows simulated measurements of v_{broad} , taking the statistical uncertainties and the floor of 5 km s⁻¹ into account. The black points in the lower left panel are the real values of v_{broad} in the sample. Different colors are used for different temperature ranges, as indicated in the legend.

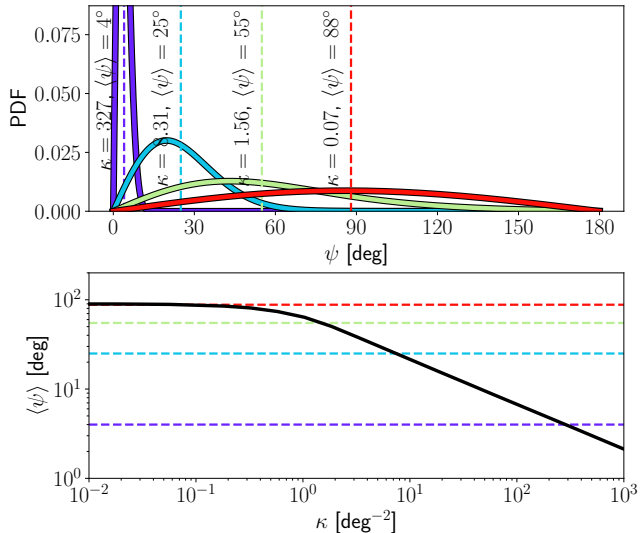


Figure 6. von-Mises Fisher distribution.

Top: The VMF distribution is exemplified for four different concentrations, quantified by both the concentration κ and the mean of ψ , $\langle\psi\rangle$. The dashed lines represent the $\langle\psi\rangle$ values. *Bottom*: How κ and $\langle\psi\rangle$ relate to one another superimposed on the four values of $\langle\psi\rangle$ from the top panel.

alignment is quantified by the concentration parameter κ . However, since the relation between κ and the width of the distribution is not straightforward, we chose to parameterize our results in terms of the mean of the spin-orbit angle ψ of the VMF distribution. For concentrated distributions, with $\kappa \gg 1$, the mean obliquity $\langle\psi\rangle \approx \kappa^{-1/2} \sqrt{\pi/2}$. For broad distributions, for which κ approaches 0, $\langle\psi\rangle \rightarrow 90^\circ$. The general relationship between κ and $\langle\psi\rangle$ was determined numerically with a Monte Carlo approach. A large number of ψ values were drawn from a VMF distribution with concentration parameter κ , the mean was calculated and recorded, and the procedure was repeated for many choices of κ . The results are shown in the bottom panel of Figure 6, relating κ to $\langle\psi\rangle$. In the top panel of the same figure, the VMF distribution is illustrated for four values of $\langle\psi\rangle$.

To specify the direction of the spin axis in three dimensions, ψ must be supplemented with an azimuthal angle Ω that specifies the direction of the component of the spin axis that is perpendicular to the orbit, following Fabrycky & Winn (2009): We assumed that Ω is uniformly distributed between 0° and 360° . Once ψ and Ω are chosen, we can calculate the sky-projected spin-orbit angle λ and the stellar inclination i using Equations 11

and 8 of Fabrycky & Winn (2009):

$$\lambda = \arctan \left(\frac{\sin \psi \sin \Omega_{sim}}{\cos \psi \sin i_o + \sin \psi \cos \Omega \cos i_o} \right)$$

$$\sin i = \frac{\sin \psi \sin \Omega}{\sin \lambda}.$$

4.4. Summary of simulation methodology

We now summarize the method by which simulated distributions of $\mathbf{v}_{\text{broad}}$ were created and compared with observations. Ultimately, the goal was to compare the observed distributions of $\langle\mathbf{v}_{\text{broad}}\rangle$ of the edge-on and face-on binaries with those of synthetic datasets that were created assuming different degrees of spin-orbit alignment. First, we determined the parameters of an empirical relationship between $v(T_{\text{eff}})$ and $\mathbf{v}_{\text{broad}}(v \sin i)$ by assuming that the primary stars in the entire sample are isotropically oriented. This was described in Sections 4.2 and 4.1. Then, we postulated a particular obliquity distribution (parameterized by $\langle\psi\rangle$) and assigned a simulated value of $\mathbf{v}_{\text{broad}}$ to each star in a sample with the following steps:

1. Assign i_o and T_{eff} values and simulate measurements of these quantities based on the reported observational uncertainties.
2. Draw ψ from a VMF distribution with the assumed value of $\langle\psi\rangle$.
3. Calculate the stellar inclination i based on the assigned i_o and ψ values.
4. Assign a rotation velocity v using the relationship $v(T_{\text{eff}})$ specified in Equation 2.
5. Calculate $v \sin i$ based on v and i .
6. Convert $v \sin i$ into $\mathbf{v}_{\text{broad}}$ using the calibrated relationship specified in Equation 1.
7. Simulate a measurement of $\mathbf{v}_{\text{broad}}$ by drawing a value from a normal distribution centered at the calculated value of $\mathbf{v}_{\text{broad}}$, and with a width equal to the uncertainty reported in Gaia DR3. The distribution was truncated at 0 km s^{-1} to prevent negative values from being drawn.
8. Whenever the result for $\mathbf{v}_{\text{broad}}$ was below 5 km s^{-1} , we repeated all the steps from the beginning to try again, since Gaia DR3 only reported $\mathbf{v}_{\text{broad}}$ when it was found to exceed 5 km s^{-1} .

The four rows of Figure 5 show snapshots in the production process of a simulated sample at steps 4, 5, 6, and 8.

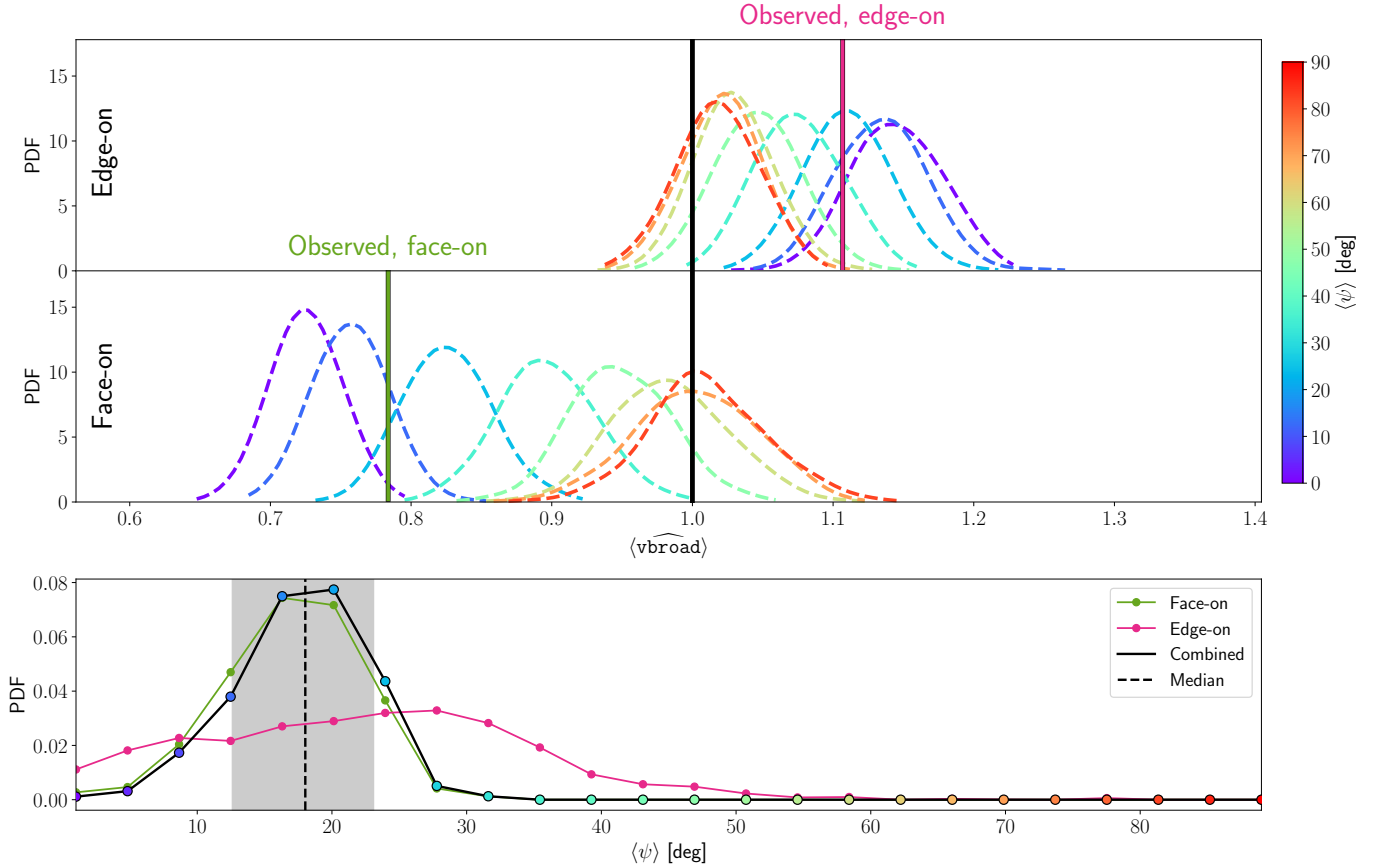


Figure 7. Edge- and face-on alignment. *Top two panels:* Each colored distribution shows the probability of making a certain measurement of $\langle \widehat{vbroad} \rangle$, given an assumed degree of spin-orbit alignment (quantified by $\langle \psi \rangle$). Vertical lines mark the observed values of $\langle \widehat{vbroad} \rangle$ across all eccentricities, for the edge-on sample (top) and the face-on sample (middle). *Bottom panel:* The posterior PDF of $\langle \psi \rangle$ derived from the edge-on (pink) and face-on (green) samples, as well as their combination (black). The results of analyzing the two subsets are compatible, and the face-on sample gives tighter constraints.

4.5. Inference of mean obliquity

To infer the spin-orbit alignment of the edge-on and face-on samples, we created synthetic samples for 25 different choices of $\langle \psi \rangle$ spaced evenly between 0° and 90° . The randomness in the simulations is due to several factors: the measurement uncertainties in i_o , \widehat{vbroad} , and T_{eff} ; the stochastic relationship between v and T_{eff} ; and the random draws of obliquities from the posited VMF distribution. Three hundred synthetic samples were created for each of the 25 values of $\langle \psi \rangle$. The simulated value of $\langle \widehat{vbroad} \rangle$ was calculated for each sample, and their distribution was taken to be the probability density for $\langle \widehat{vbroad} \rangle$ for the given value of $\langle \psi \rangle$. See the dashed and colored lines in Figure 7. We used these probability density functions to calculate the posterior probability density function of $\langle \psi \rangle$ given the observed value of $\langle \widehat{vbroad} \rangle$.

5. RESULTS

First, we analyzed the full sample, regardless of orbital eccentricity. We expect the spin-orbit distributions of the edge-on and face-on binaries to be indistinguishable, because there should be no dependence of a system's intrinsic geometry on the direction from which it is viewed. Figure 7 displays the results. In the top two panels, the observed values of $\langle \widehat{vbroad} \rangle$ are shown as vertical lines. Alongside them are dashed colored curves that were constructed from the synthetic versions of the same samples. Each color represents the probability of measuring $\langle \widehat{vbroad} \rangle$ for a given value of $\langle \psi \rangle$. The bottom panel shows the posterior PDFs for $\langle \psi \rangle$ as informed by the face-on binaries (green), edge-on binaries (pink), and the entire sample (black). The results from the edge-on and face-on samples are consistent, as expected, and indicate $\langle \psi \rangle = 18 \pm 5^\circ$. Thus, the binaries as a whole show a moderate degree of spin-orbit alignment.

Next, motivated by the experiments on eccentricity described in Section 3 and displayed in Figure 3, we divided the sample into 5 subsamples according to ec-

centricity, and performed the preceding analysis on each subsample. The eccentricity ranges that defined the bins were $[0 - 0.15)$, $[0.15 - 0.30)$, $[0.30 - 0.50)$, $[0.50 - 0.70)$, and $[0.70 - 1]$. The number of binaries in each eccentricity bin was 568, 729, 780, 474, and 176, respectively.

Figure 8 shows the results, combining the information from the face-on and edge-on systems for the five eccentricity bins. Systems with eccentricities below 0.15 have an obliquity distribution consistent with perfect alignment. As eccentricity increases, the obliquity dispersion also increases. Systems with eccentricities above 0.7 have a mean obliquity of $\langle \psi \rangle = 46_{-24}^{+26}^\circ$.

5.1. Caveats and robustness of the result

A potential source of systematic error is the unmodelled effect of light from the secondary star in each binary on the determination of $\mathbf{v}_{\text{broad}}$ from the RVS spectra. Any bias in $\mathbf{v}_{\text{broad}}$ due to the secondary star might depend on orbital inclination, because the line-of-sight component of the orbital motion is higher for an edge-on system than for a face-on system. In addition, a significant contribution of light from the secondary star would probably lead to an increase in the reported uncertainty of $\mathbf{v}_{\text{broad}}$, because the uncertainty reported in Gaia DR3 is based on the standard deviation of the time series of individual $\mathbf{v}_{\text{broad}}$ measurements. We did not find any systematic difference in the distribution of $\mathbf{v}_{\text{broad}}$ uncertainties between the face-on and edge-on systems. Regardless, in an attempt to exclude the most problematic systems, we required a stringent upper limit of 10 km s^{-1} on the uncertainty of $\mathbf{v}_{\text{broad}}$.

We also need to remind ourselves that the stellar inclination derived from $v \sin i$ is subject to a discrete degeneracy; we cannot distinguish i from $180^\circ - i$. If the true obliquity distribution of the binary systems is well approximated by the VMF distribution, then our results are probably not affected much by this degeneracy. However, if the real probability distribution does not decline monotonically with ψ and has an excess of retrograde systems, then the degeneracy might be serious. For example, if the true obliquity distribution were bimodal with peaks near both $\psi = 0^\circ$ and $\psi = 180^\circ$, then our method would falsely infer that the distribution is only concentrated near 0° . The degeneracy in the stellar inclination can be broken, in principle, through interferometric observations (see Albrecht et al. 2022 and references therein).

Finally, we note that the results of analyzing the edge-on and face-on subsets are consistent with each other. However, the most powerful constraints come from the face-on subset with low-eccentricity orbits. This is because the main observational implication of spin-orbit

alignment is that $\sin i$ should be systematically low for face-on systems. For face-on systems, i is low and $\sin i \approx i$. Therefore any change in i leads a proportional change in $\sin i$. For edge-on systems, $i \approx \pi/2$ and $\sin i \approx 1 - \alpha^2/2$ where $\alpha = \pi/2 - i$. Therefore, a change in i leads to only a second-order change in $\sin i$. The effects of this flattening of the sine function with i is familiar from similar studies of stars with transiting planets (see, e.g., Winn et al. 2017), and causes face-on samples to bear most of the statistical power when constraining the well-aligned systems. The advantage of face-on systems over edge-on systems is reduced for samples with larger spin-orbit misalignments, and reversed for nearly polar orbits.

6. DISCUSSION

We have found that in binaries with F-type primaries and periods between 50 and 1000 days, spin-orbit misalignment of the primary star is associated with high orbital eccentricity. Dissipative tidal interactions between the two stars would naturally lead to both spin-orbit alignment and orbital circularization. However, with periods exceeding 50 days, we would not expect ongoing tidal interactions to be significant (see, e.g., Justesen & Albrecht 2021; Bashi et al. 2023). Tidal dissipation would have been more rapid early in the stars' lives when they were larger and still contracting onto the main sequence. But the absence of a detectable dependence of $\mathbf{v}_{\text{broad}}$ (and by extension, v) on orbital period suggests that alignment and synchronization of the stellar spin is not the dominant factor in shaping the stellar obliquities in our sample.

Instead, the eccentricity-obliquity correlation may have been imprinted during formation of these binaries (see Offner et al. 2023 for an extensive discussion of stellar binary formation). To begin, while in-situ formation of stellar binaries via the fragmentation of turbulent molecular cores has been invoked to explain eccentricity statistics of wider stellar binaries (Xu et al. 2023), such a process is not thought to efficiently form stellar binaries with separations $\lesssim 10^2$ au (e.g. Guszejnov et al. 2017; Offner et al. 2023). In order to form binaries with periods comparable to those in our sample, three classes of theories can be invoked: capture from an unbound state, gas-driven migration from an initially wider orbit, and secular processes induced by a distant tertiary companion (Offner et al. 2023). In the first case, sufficiently dense stellar environments can yield compact binaries (separations \lesssim au) via gravitational capture and even partner exchange (e.g. Dorval et al. 2017), though such processes may not be as efficient in gas-rich environments (e.g. Wall et al. 2019). Naively,

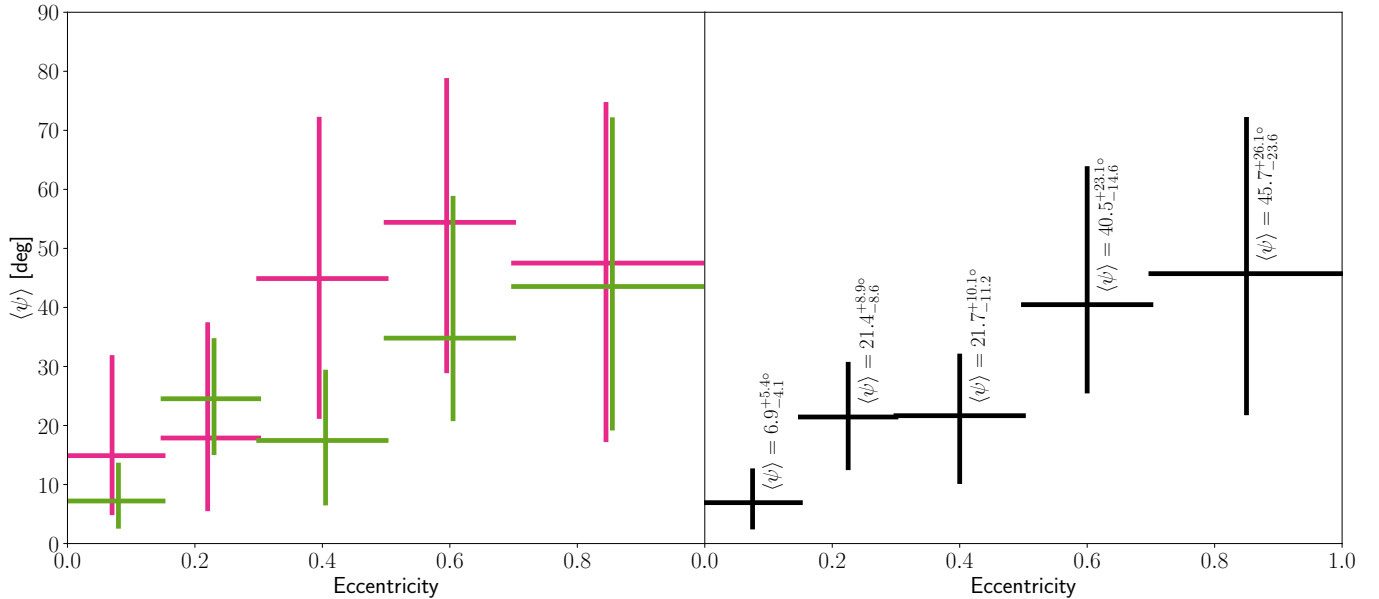


Figure 8. High obliquities are associated with high orbital eccentricity. The results for the spin-orbit alignment of our binary star sample are shown as a function of eccentricity in five bins. The eccentricity ranges are indicated by horizontal bars and vertical bars represent the one-sigma confidence intervals for $\langle\psi\rangle$. Pink, green and black signify edge-on, face-on, and combined results, respectively. The green error bars were displaced slightly to the right to avoid overlapping with the pink error bars.

such dynamically violent processes should not produce many circular binaries with low obliquities, though they may be responsible for the eccentric, misaligned binaries in our sample. In the second case, gas-driven migration has classically been thought to result in binary coalescence (Artymowicz & Lubow 1996), though recent studies have concluded that the evolution of the binary separation and eccentricity may be more complex than previously thought (see e.g. Lai & Muñoz 2023 for a review), and a direct theoretical prediction for the binary properties at the end of such a process is uncertain. Finally, in the third scenario, a tertiary companion may induce oscillations of the eccentricity in the binary system and the mutual inclination between the binary system and the tertiary system via the von Zeipel-Lidov-Kozai effect (von Zeipel 1910; Lidov 1962; Kozai 1962). Such oscillations, in conjunction with standard theories of tidal dissipation, can efficiently form binaries with periods $\lesssim 10$ days (Fabrycky & Tremaine 2007), but are unlikely to form the wider binaries in our sample, where tidal dissipation is inefficient.

In summary, while the formation of binaries with the orbital periods considered in our sample is still not well understood, the most promising mechanisms involve dynamical processes that should often lead to eccentric and misaligned binaries.

Separately, a possible suspect for the observed correlation is the interaction of a binary with a third star

or multiple stars in the birth cluster after its formation. Starting from a low-obliquity, low-eccentricity state, such gravitational interactions would tend to excite both the binary’s orbital eccentricity (e.g. Heggie & Rasio 1996) and its orbital inclination (e.g. Rodet et al. 2021). Close encounters with other stars or multiple star systems could lead to scattering events that change the velocity vector of one star in the binary and therefore change both orbital eccentricity as well as the orbital plane.

Under this hypothesis, one might expect that more closely bound systems with shorter orbital periods would be more protected and would display lower obliquities and eccentricities. We do not see a clear trend with period for eccentricity and obliquities. Additionally, for the short periods of binaries considered here, the rate of encounters sufficiently strong to affect the orbit ($\sim 1 \text{ Gyr}^{-1}$, e.g. Rodet et al. 2021) is likely too slow to affect the binary orbit within characteristic birth cluster lifetimes ($\sim 10 \text{ Myr}$, e.g. Lamers et al. 2005), though this comparison depends on the highly uncertain properties of stellar birth clusters and the age of the cluster at the time of any dynamical interaction.

Our results can also be compared to measurements of the obliquities of single stars with known planetary systems. It appears as if the alignment of the low-eccentricity binaries in our sample is comparable to that of the most well-aligned hot Jupiter systems (Albrecht

et al. 2022) as well as most of the stars hosting compact multi-transiting planetary systems (Kundstrup et al., under review). It also seems to be consistent with the good alignment of the Sun with respect to the orbital planes of the planets in the Solar System.

Future studies might be able to test if the above processes or other processes lead naturally to the observed distribution of spin-orbit angles and its dependence on eccentricity. This will be possible not only because the number of systems is expected to increase with DR4. The longer time baseline (DR3 included 34 months of data) will allow for longer period systems to be included. DR4 will also contain epoch astrometry and RVS spectra. In particular, the epoch RVS data allows for the inclusion of SB2 binaries, thereby extending the mass ratio range. The DR4 data will also be sensitive to lower mass secondaries. Future studies might also test for any age dependency. Using samples like the one presented by Hwang (2023) will also allow the study of systems with significantly larger separations and allow an investigation of the role multiplicity. Higher spectral resolution for lower temperature systems should allow us to probe systems with stars outside the spectral range probed here. For example APOGEE (Abdurro'uf et al. 2022) and GALAH (Buder et al. 2021) spectra have more than twice the resolution of Gaia RVS spectra, whereas single object high resolution echelle spectrographs have resolutions of about an order of magnitude higher. Finally, our methodology could be further developed including e.g. ages and metallicity into the rotation modeling as well as employing a hierarchical approach for obliquity and model parameter inference.

This research benefited from using the Gaiachatbot at <https://gaiachat.streamlit.app/> provided by Veridicity.

This work has made use of data from the European Space Agency (ESA) mission *Gaia* (<https://www.cosmos.esa.int/gaia>), processed by the *Gaia* Data Processing and Analysis Consortium (DPAC, <https://www.cosmos.esa.int/web/gaia/dpac/consortium>). Funding for the DPAC has been provided by national institutions, in particular the institutions participating in the *Gaia* Multilateral Agreement.

We acknowledge the support from the Danish Council for Independent Research through a grant, No.2032-00230B.

This work was supported by a research grant (42101) from VILLUM FONDEN as well as The Independent Research Fund Denmark's Inge Lehmann program (grant agreement No. 1131-00014B).

This project has received funding from the European Union's Horizon 2020 research and innovation programme under grant agreement No 101004719 (ORP: OPTICON RadioNet Pilot)

S.H.A. thanks the Department of Astrophysical Sciences at Princeton University and the Action Station chef of the faculty lunch room at Prospect House for their hospitality during a sabbatical stay during which part of the work for this project was conducted.

Facilities: NOT (Djupvik & Andersen 2010), Gaia (Gaia Collaboration et al. 2016)

Software: iSpec (Blanco-Cuaresma et al. 2014)

REFERENCES

- Abdurro'uf, Accetta, K., Aerts, C., et al. 2022, ApJS, 259, 35, doi: [10.3847/1538-4365/ac4414](https://doi.org/10.3847/1538-4365/ac4414)
- Albrecht, S., Reffert, S., Snellen, I., Quirrenbach, A., & Mitchell, D. S. 2007, A&A, 474, 565, doi: [10.1051/0004-6361:20077953](https://doi.org/10.1051/0004-6361:20077953)
- Albrecht, S., Reffert, S., Snellen, I. A. G., & Winn, J. N. 2009, Nature, 461, 373, doi: [10.1038/nature08408](https://doi.org/10.1038/nature08408)
- Albrecht, S., Setiawan, J., Torres, G., Fabrycky, D. C., & Winn, J. N. 2013, ApJ, 767, 32, doi: [10.1088/0004-637X/767/1/32](https://doi.org/10.1088/0004-637X/767/1/32)
- Albrecht, S., Winn, J. N., Carter, J. A., Snellen, I. A. G., & de Mooij, E. J. W. 2011, ApJ, 726, 68, doi: [10.1088/0004-637X/726/2/68](https://doi.org/10.1088/0004-637X/726/2/68)
- Albrecht, S., Winn, J. N., Torres, G., et al. 2014a, ApJ, 785, 83, doi: [10.1088/0004-637X/785/2/83](https://doi.org/10.1088/0004-637X/785/2/83)
- . 2014b, ApJ, 785, 83, doi: [10.1088/0004-637X/785/2/83](https://doi.org/10.1088/0004-637X/785/2/83)
- Albrecht, S. H., Dawson, R. I., & Winn, J. N. 2022, arXiv e-prints, arXiv:2203.05460, <https://arxiv.org/abs/2203.05460>
- Anderson, K. R., & Lai, D. 2021, ApJ, 906, 17, doi: [10.3847/1538-4357/abca2](https://doi.org/10.3847/1538-4357/abca2)
- Anderson, K. R., Lai, D., & Storch, N. I. 2017, MNRAS, 467, 3066, doi: [10.1093/mnras/stx293](https://doi.org/10.1093/mnras/stx293)
- Artymowicz, P., & Lubow, S. H. 1996, ApJL, 467, L77, doi: [10.1086/310200](https://doi.org/10.1086/310200)
- Ball, W. H., Triaud, A. H. M. J., Hatt, E., Nielsen, M. B., & Chaplin, W. J. 2023, MNRAS, 521, L1, doi: [10.1093/mnras/slado12](https://doi.org/10.1093/mnras/slado12)
- Bashi, D., Mazeh, T., & Faigler, S. 2023, MNRAS, 522, 1184, doi: [10.1093/mnras/stad999](https://doi.org/10.1093/mnras/stad999)
- Bate, M. R. 2018, MNRAS, 475, 5618, doi: [10.1093/mnras/sty169](https://doi.org/10.1093/mnras/sty169)

- Bate, M. R., Lodato, G., & Pringle, J. E. 2010, *MNRAS*, 401, 1505, doi: [10.1111/j.1365-2966.2009.15773.x](https://doi.org/10.1111/j.1365-2966.2009.15773.x)
- Blanco-Cuaresma, S., Soubiran, C., Jofré, P., & Heiter, U. 2014, in *Astronomical Society of India Conference Series*, Vol. 11, *Astronomical Society of India Conference Series*, 85–91, doi: [10.48550/arXiv.1312.4545](https://doi.org/10.48550/arXiv.1312.4545)
- Buder, S., Sharma, S., Kos, J., et al. 2021, *MNRAS*, 506, 150, doi: [10.1093/mnras/stab1242](https://doi.org/10.1093/mnras/stab1242)
- Djupvik, A. A., & Andersen, J. 2010, in *Astrophysics and Space Science Proceedings*, Vol. 14, *Highlights of Spanish Astrophysics V*, 211, doi: [10.1007/978-3-642-11250-8_21](https://doi.org/10.1007/978-3-642-11250-8_21)
- Dorval, J., Boily, C. M., Moraux, E., & Roos, O. 2017, *MNRAS*, 465, 2198, doi: [10.1093/mnras/stw2880](https://doi.org/10.1093/mnras/stw2880)
- Eggleton, P. P., & Kiseleva-Eggleton, L. 2001, *ApJ*, 562, 1012, doi: [10.1086/323843](https://doi.org/10.1086/323843)
- Fabrycky, D., & Tremaine, S. 2007, *ApJ*, 669, 1298, doi: [10.1086/521702](https://doi.org/10.1086/521702)
- Fabrycky, D. C., & Winn, J. N. 2009, *ApJ*, 696, 1230, doi: [10.1088/0004-637X/696/2/1230](https://doi.org/10.1088/0004-637X/696/2/1230)
- Fielding, D. B., McKee, C. F., Socrates, A., Cunningham, A. J., & Klein, R. I. 2015, *MNRAS*, 450, 3306, doi: [10.1093/mnras/stv836](https://doi.org/10.1093/mnras/stv836)
- Frémat, Y., Royer, F., Marchal, O., et al. 2023, *A&A*, 674, A8, doi: [10.1051/0004-6361/202243809](https://doi.org/10.1051/0004-6361/202243809)
- Gaia Collaboration, Prusti, T., de Bruijne, J. H. J., et al. 2016, *A&A*, 595, A1, doi: [10.1051/0004-6361/201629272](https://doi.org/10.1051/0004-6361/201629272)
- Gaia Collaboration, Brown, A. G. A., Vallenari, A., et al. 2021, *A&A*, 649, A1, doi: [10.1051/0004-6361/202039657](https://doi.org/10.1051/0004-6361/202039657)
- Gaia Collaboration, Arenou, F., Babusiaux, C., et al. 2022, *arXiv e-prints*, arXiv:2206.05595, doi: [10.48550/arXiv.2206.05595](https://doi.org/10.48550/arXiv.2206.05595)
- Glebocki, R., & Stawikowski, A. 1997, *A&A*, 328, 579
- Guszejnov, D., Hopkins, P. F., & Krumholz, M. R. 2017, *MNRAS*, 468, 4093, doi: [10.1093/mnras/stx725](https://doi.org/10.1093/mnras/stx725)
- Halbwachs, J.-L., Pourbaix, D., Arenou, F., et al. 2023, *A&A*, 674, A9, doi: [10.1051/0004-6361/202243969](https://doi.org/10.1051/0004-6361/202243969)
- Hale, A. 1994, *AJ*, 107, 306, doi: [10.1086/116855](https://doi.org/10.1086/116855)
- Heggie, D. C., & Rasio, F. A. 1996, *MNRAS*, 282, 1064, doi: [10.1093/mnras/282.3.1064](https://doi.org/10.1093/mnras/282.3.1064)
- Howe, K. S., & Clarke, C. J. 2009, *MNRAS*, 392, 448, doi: [10.1111/j.1365-2966.2008.14073.x](https://doi.org/10.1111/j.1365-2966.2008.14073.x)
- Hwang, H.-C. 2023, *MNRAS*, 518, 1750, doi: [10.1093/mnras/stac3116](https://doi.org/10.1093/mnras/stac3116)
- Jennings, R. M., & Chiang, E. 2021, *MNRAS*, 507, 5187, doi: [10.1093/mnras/stab2429](https://doi.org/10.1093/mnras/stab2429)
- Justesen, A. B., & Albrecht, S. 2019, *A&A*, 625, A59, doi: [10.1051/0004-6361/201834368](https://doi.org/10.1051/0004-6361/201834368)
- . 2020, *A&A*, 642, A212, doi: [10.1051/0004-6361/202039138](https://doi.org/10.1051/0004-6361/202039138)
- . 2021, *ApJ*, 912, 123, doi: [10.3847/1538-4357/abefcd](https://doi.org/10.3847/1538-4357/abefcd)
- Kozai, Y. 1962, *AJ*, 67, 591, doi: [10.1086/108790](https://doi.org/10.1086/108790)
- Kraft, R. P. 1967, *ApJ*, 150, 551, doi: [10.1086/149359](https://doi.org/10.1086/149359)
- Lai, D., & Muñoz, D. J. 2023, *ARA&A*, 61, 517, doi: [10.1146/annurev-astro-052622-022933](https://doi.org/10.1146/annurev-astro-052622-022933)
- Lamers, H. J. G. L. M., Gieles, M., & Portegies Zwart, S. F. 2005, *A&A*, 429, 173, doi: [10.1051/0004-6361:20041476](https://doi.org/10.1051/0004-6361:20041476)
- Lehmann, H., Southworth, J., Tkachenko, A., & Pavlovski, K. 2013, *A&A*, 557, A79, doi: [10.1051/0004-6361/201321400](https://doi.org/10.1051/0004-6361/201321400)
- Lidov, M. L. 1962, *Planet. Space Sci.*, 9, 719, doi: [10.1016/0032-0633\(62\)90129-0](https://doi.org/10.1016/0032-0633(62)90129-0)
- Louden, E. M., Winn, J. N., Petigura, E. A., et al. 2021, *AJ*, 161, 68, doi: [10.3847/1538-3881/abcebd](https://doi.org/10.3847/1538-3881/abcebd)
- Marcussen, M. L., & Albrecht, S. H. 2022, *ApJ*, 933, 227, doi: [10.3847/1538-4357/ac75c2](https://doi.org/10.3847/1538-4357/ac75c2)
- Masuda, K., & Winn, J. N. 2020, *AJ*, 159, 81, doi: [10.3847/1538-3881/ab65be](https://doi.org/10.3847/1538-3881/ab65be)
- Mazeh, T., & Shaham, J. 1979, *A&A*, 77, 145
- Naoz, S., & Fabrycky, D. C. 2014, *ApJ*, 793, 137, doi: [10.1088/0004-637X/793/2/137](https://doi.org/10.1088/0004-637X/793/2/137)
- Offner, S. S. R., Dunham, M. M., Lee, K. I., Arce, H. G., & Fielding, D. B. 2016, *ApJL*, 827, L11, doi: [10.3847/2041-8205/827/1/L11](https://doi.org/10.3847/2041-8205/827/1/L11)
- Offner, S. S. R., Moe, M., Kratter, K. M., et al. 2023, in *Astronomical Society of the Pacific Conference Series*, Vol. 534, *Protostars and Planets VII*, ed. S. Inutsuka, Y. Aikawa, T. Muto, K. Tomida, & M. Tamura, 275, doi: [10.48550/arXiv.2203.10066](https://doi.org/10.48550/arXiv.2203.10066)
- Pavlovski, K., Southworth, J., & Kolbas, V. 2011, *ApJL*, 734, L29, doi: [10.1088/2041-8205/734/2/L29](https://doi.org/10.1088/2041-8205/734/2/L29)
- Philippov, A. A., & Rafikov, R. R. 2013, *ApJ*, 768, 112, doi: [10.1088/0004-637X/768/2/112](https://doi.org/10.1088/0004-637X/768/2/112)
- Rodet, L., Su, Y., & Lai, D. 2021, *ApJ*, 913, 104, doi: [10.3847/1538-4357/abf8a7](https://doi.org/10.3847/1538-4357/abf8a7)
- Schlaufman, K. C. 2010, *ApJ*, 719, 602, doi: [10.1088/0004-637X/719/1/602](https://doi.org/10.1088/0004-637X/719/1/602)
- Sybilski, P., Pawłaszek, R. K., Sybilaska, A., et al. 2018, *MNRAS*, 478, 1942, doi: [10.1093/mnras/sty1135](https://doi.org/10.1093/mnras/sty1135)
- Thies, I., Kroupa, P., Goodwin, S. P., Stamatellos, D., & Whitworth, A. P. 2011, *MNRAS*, 417, 1817, doi: [10.1111/j.1365-2966.2011.19390.x](https://doi.org/10.1111/j.1365-2966.2011.19390.x)
- TriAUD, A. H. M. J., Hebb, L., Anderson, D. R., et al. 2013, *A&A*, 549, A18, doi: [10.1051/0004-6361/201219643](https://doi.org/10.1051/0004-6361/201219643)
- von Zeipel, H. 1910, *Astronomische Nachrichten*, 183, 345
- Wall, J. E., McMillan, S. L. W., Mac Low, M.-M., Klessen, R. S., & Portegies Zwart, S. 2019, *ApJ*, 887, 62, doi: [10.3847/1538-4357/ab4db1](https://doi.org/10.3847/1538-4357/ab4db1)
- Weis, E. W. 1974, *ApJ*, 190, 331, doi: [10.1086/152881](https://doi.org/10.1086/152881)
- Winn, J. N., Petigura, E. A., Morton, T. D., et al. 2017, *AJ*, 154, 270, doi: [10.3847/1538-3881/aa93e3](https://doi.org/10.3847/1538-3881/aa93e3)

Xu, S., Hwang, H.-C., Hamilton, C., & Lai, D. 2023, ApJL, 949, L28, doi: [10.3847/2041-8213/acd6f7](https://doi.org/10.3847/2041-8213/acd6f7)

Zhou, G., & Huang, C. X. 2013, ApJL, 776, L35, doi: [10.1088/2041-8205/776/2/L35](https://doi.org/10.1088/2041-8205/776/2/L35)